Polaritonic Chern Insulators in Monolayer Semiconductors

Li He,[1] Jingda Wu[ORCID],[2] Jicheng Jin,[1] Eugene J. Mele[ORCID],[1] and Bo Zhen[ORCID][1,*]

[1]*Department of Physics and Astronomy, University of Pennsylvania, Philadelphia, Pennsylvania 19104, USA*
[2]*Department of Physics and Astronomy, University of British Columbia, Vancouver, British Columbia V6T 1Z1, Canada*

Systems with strong light-matter interaction open up new avenues for studying topological phases of matter. Examples include exciton polaritons, mixed light-matter quasiparticles, where the topology of the polaritonic band structure arises from the collective coupling between matter wave and optical fields strongly confined in periodic dielectric structures. Distinct from light-matter interaction in a uniform environment, the spatially varying nature of the optical fields leads to a fundamental modification of the well-known optical selection rules, which were derived under the plane wave approximation. Here we identify polaritonic Chern insulators by coupling valley excitons in transition metal dichalcogenides to photonic Bloch modes in a dielectric photonic crystal slab. We show that polaritonic Dirac points, which are markers for topological phase transition points, can be constructed from the collective coupling between valley excitons and photonic Dirac cones in the presence of both time-reversal and inversion symmetries. Lifting exciton valley degeneracy by breaking time-reversal symmetry leads to gapped polaritonic bands with nonzero Chern numbers. Through numerical simulations, we predict polaritonic chiral edge states residing inside the topological gaps. Our Letter paves the way for the further study of strong exciton-photon interaction in nanophotonic structures and for exploring polaritonic topological phases and their practical applications in polaritonic devices.

Introduction.—Strongly coupling photons to excitonic resonances in semiconductors gives rise to new elementary excitations, exciton polaritons. These quasiparticles combine the properties of their parental photon and matter components and thereby provide an ideal platform to study quantum many-body physics, including Bose-Einstein condensates [1], superfluidity [2], and Berezinskii-Kosterlitz-Thouless transition [3]. Motivated by the recent rapid progress in topological band theory [4–6], there has been great interest in applying it to polaritonic systems and exploring novel topological phenomena intrinsic to exciton polaritons [7–13]. For example, in contrast to photons that rarely interact with each other, exciton polaritons exhibit strong nonlinearities through exciton-exciton interactions [14–16], allowing for the study of nonlinear and interacting topological phenomena [6]. Another particularly promising perspective of exciton polaritons is the possibility of breaking time-reversal symmetry (T) via the excitonic component, opening the door to the realization of a range of T-broken topological phases [5,17] at optical frequencies, such as Chern insulators with protected unidirectional modes on the edges [5,6]. By contrast, exploring such topological phenomena in purely photonic systems remains challenging due to the lack of an efficient method to break T for photons.

Recently, various topological exciton-polariton states have been theoretically proposed [7–10] and experimentally studied in the solid-state setting by embedding semiconductor quantum wells into lattices of coupled microcavities [11] or transferring two-dimensional transition metal dichalcogenides (TMDs) onto dielectric photonic crystal slabs [12,13]. However, exciton-photon interaction in such periodic structures, which underlies the topology of the resulting polaritonic band structures, has neglected the periodic modulation of the refractive index and the spatially varying field strength and polarization [18]—a feature unique for strongly confined optical fields. The nonuniform distribution of polarization—local transverse photon spin—completely modifies the optical selection rules in light-matter interaction derived under the assumption of a plane wave excitation with a single polarization [19]. As a result, a comprehensive understanding of the light-matter interaction in periodic structures is expected to change the topological properties of the exciton polaritons in a fundamental way.

Here, we present theoretical investigations of exciton polaritons formed by strongly coupling monolayer TMDs to a photonic crystal slab and show how the modified optical selection rules in nanophotonic structures can lead to exciton polaritons with new bulk topology when the time-reversal symmetry is broken through the exciton components. We start by deriving the effective Hamiltonian that captures the optical selection rules in periodic structures near high-symmetry momentum (**k**) points. Based on that, we show the polaritonic Dirac points can be constructed by coupling exciton resonances to photonic Dirac points. Similar to electronic and photonic systems, polaritonic Dirac points

are also protected by the product of inversion (P) and time-reversal symmetry. As a result, breaking T while preserving P gaps out polariton Dirac points, leading to polaritonic bands with nontrivial Chern numbers. We validate the topological polaritonic band structures through finite-difference time-domain (FDTD) simulations. All calculations are based on realistic material parameters [20,21], which makes our predictions immediately applicable for experimental realization.

Results.—We start by introducing the concept of collective coupling between exciton resonances in a TMD monolayer and photonic Bloch modes in a dielectric photonic crystal slab. One crucial feature of exciton-polariton systems is the significant size mismatch between the periodic potentials for photons and excitons [Fig. 1(a)]: the photonic unit cell ($a \sim 300$ nm) is orders of magnitude larger than its excitonic counterpart ($a_X \sim 0.3$ nm). Accordingly, to study the exciton-polariton dispersions that are defined in the photonic Brillouin zone (BZ), one needs to fold the free exciton dispersion back into the photonic BZ, leading to highly degenerate excitonic bands with N-fold near degeneracy, where $N \gg 1$. Note that here, due to the significant size mismatch, we neglect exciton band dispersion and assume it to be flat. The dispersionless and degenerate exciton bands in momentum space are equivalent to an ensemble of noninteracting local exciton states in real space. The coupling between N degenerate exciton modes and a single photon mode is described by the Tavis-Cummings Hamiltonian [22], a matrix of $N + 1$ dimensions, as follows:

$$H_k = \omega_p(k)a_k^\dagger a_k$$
$$+ \sum_i^N [\omega_X b_{k,i}^\dagger b_{k,i} + g_i(k)a_k^\dagger b_{k,i} + g_i^*(k)b_{k,i}^\dagger a_k], \quad (1)$$

(a) Real space   (b) k space

$a_X \sim 0.3$nm

UP

Dark states

LP
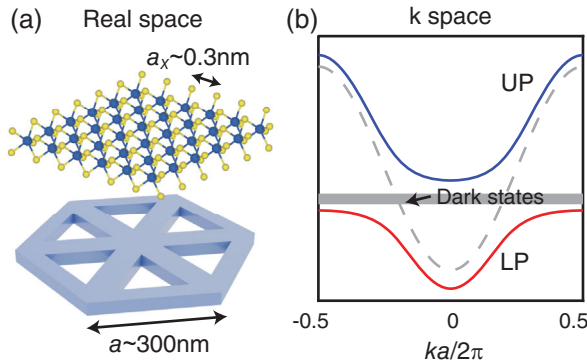
$a \sim 300$nm

-0.5   0   0.5
$ka/2\pi$

FIG. 1. Collective exciton-photon coupling in the TMD-PhC system. (a) Schematics of a TMD monolayer placed on top of a dielectric PhC slab. (b) Upper (blue) and lower (red) polariton branches arise from the collective coupling between a photon band (dashed parabola) and N-fold degenerate exciton bands. There are also $N - 1$ exciton bands (shaded in gray) in the polariton gap that are decoupled from the photon band.

where $a_k^\dagger$ and $b_{k,i}^\dagger$ are creation operators for photon and ith exciton modes, with wave vector k and eigenenergies ω_p and ω_X, respectively. The coefficient g_i denotes the coupling strength between the ith exciton mode and the photon mode. As shown in Fig. 1(b), in the strong coupling regime, exciton modes collectively couple to the photon mode, leading to two "bright" polariton branches, namely, the upper and lower polariton bands, with eigenvalues of $E_\pm = (\frac{\omega_p + \omega_X}{2}) \pm \frac{1}{2}\sqrt{(\omega_p - \omega_X)^2 + 4\sum_i^N |g_i|^2}$. In addition, there are $N - 1$ "dark" exciton modes at the original exciton energy ω_X, residing inside the polariton gap, as they are completely decoupled from the photon mode. The fact that the photon mode only mixes with a linear superposition of exciton modes is a direct consequence of the degeneracy in exciton energies, similar to the superradiance phenomenon in the context of quantum electrodynamics: an ensemble of noninteracting emitters couple to a common electromagnetic field through the formation of a collective mode [23]. In general, when an ensemble of exciton states couple to N_p photon modes, the number of bright polariton bands is $N_{\text{polariton}} = N_p(N_X + 1)$, where N_X here represents the number of distinct excitonic energies, while not taking into account the degrees of freedom (e.g., valley) within energy degeneracies. In the simplest example above, $N_X = 1$, $N_p = 1$, and $N_{\text{polariton}} = 2$.

Next, we show how polaritonic Dirac points can be constructed by collectively coupling valley excitons in TMDs to photonic Dirac points. As a concrete example, we consider a Si_3N_4 photonic crystal (PhC) slab ($n = 2.02$, thickness 230 nm) with a honeycomb lattice of triangular holes [Fig. 2(a)], which hosts photonic Dirac points at the K/K' corners of the photonic BZ [24]. The two degenerate photonic modes at the Dirac points can be characterized by their threefold rotation (C_3) eigenvalues $c_3^\pm = e^{\pm i2\pi/3}$. For simplicity, we further assume that the energy of the TMD valley excitons $\omega_{K/K'}$ is on resonance with the photonic Dirac point ω_p. This is not an essential simplification since a small energy detuning will not qualitatively modify the polaritonic dispersion and the polariton Dirac points present below will remain (see Supplemental Material [25]). We can then represent the polariton wave functions using a six-component spinor $\Psi = (|p^+\rangle, |K^+\rangle, |K'^+\rangle, |p^-\rangle, |K^-\rangle, |K'^-\rangle)$ and write down the low-energy Hamiltonian near the K point of the photonic BZ as follows:

$$H_{\mathbf{k}} = \begin{bmatrix} \omega_p & \alpha & \beta & v(k_x - ik_y) & 0 & 0 \\ \alpha^* & \omega_K & 0 & 0 & 0 & 0 \\ \beta^* & 0 & \omega_{K'} & 0 & 0 & 0 \\ v(k_x + ik_y) & 0 & 0 & \omega_p & \beta^* & \alpha^* \\ 0 & 0 & 0 & \beta & \omega_K & 0 \\ 0 & 0 & 0 & \alpha & 0 & \omega_{K'} \end{bmatrix}. \quad (2)$$
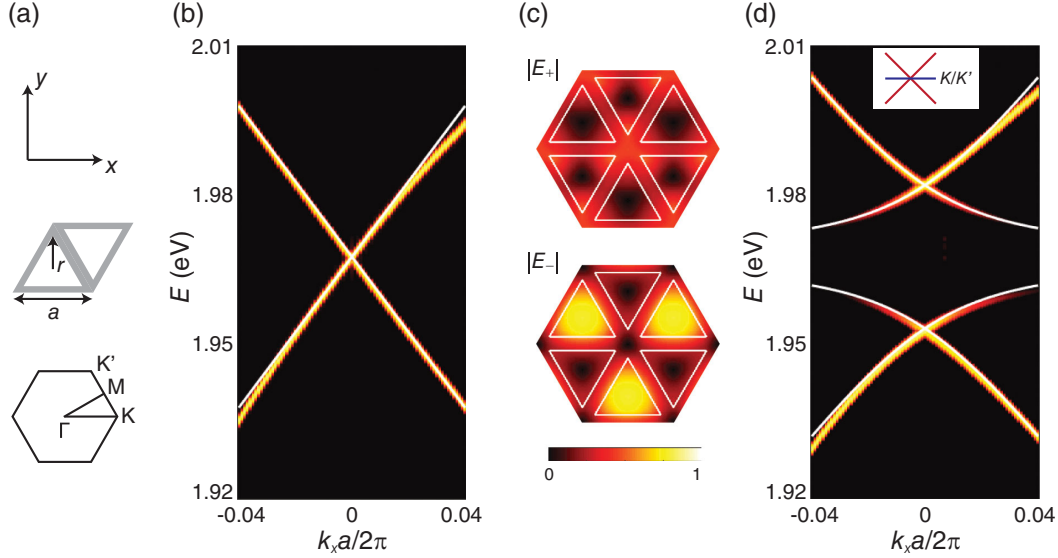
FIG. 2. Polaritonic Dirac points resulting from coupling valley excitons to a photonic Dirac point. (a) Si_3N_4 PhC slab with a honeycomb lattice of triangular holes (lattice constant $a = 310$ nm, hole radius $r = 130$ nm). (b) Calculated photonic band structure showing a Dirac cone near the K point. (c) Decomposition of the $|p^+\rangle$ photon mode into two circular polarizations of $E_\pm = (E_x \pm iE_y)/\sqrt{2}$. The inequivalent distributions of $|E_\pm|$ imply distinct coupling strengths between $|p^+\rangle$ and excitons in K/K' valleys. (d) Exciton-photon coupling generates a pair of polaritonic Dirac cones. White lines are the analytical results obtained from the effective Hamiltonian.

Here $\mathbf{k}$ is the wave vector measured relative to the photonic K point. $|p^\pm\rangle$ are the two degenerate photon modes at the photonic Dirac point. $|K^\pm\rangle$ and $|K'^\pm\rangle$ are the collective exciton modes formed by K and K' valley excitons with eigenvalues of $c_3^\pm$, respectively. Notably, the lack of continuous translation symmetry in PhCs gives rise to spatially varying field polarization in a photonic unit cell [Fig. 2(c)], which, in turn, leads to different coupling strengths ($|\alpha| \neq |\beta|$) between valley excitons and a fixed photon mode. Moreover, neither of the valley excitons are completely decoupled from the photon mode as $|\alpha, \beta| \sim \sqrt{\int_{\mathrm{unit\,cell}} dx dy |E_\pm|^2} > 0$, where $E_\pm = (E_x \pm iE_y)/\sqrt{2}$ is the electric fields of $|p^+\rangle$ photon mode decomposed into the circular basis. This is to be distinguished from previous studies on semiconductor exciton polaritons where the optical modes are approximated as plane waves and thus a fixed photon mode only couples to excitons of one particular spin [9,11]. In the presence of time-reversal symmetry, K and K' valley excitons are degenerate in energy ($\omega_K = \omega_{K'}$ and $N_X = 1$). Consequently, the hybridization of excitons and photons generates $2 \times (1 + 1) = 4$ polariton bands that are doubly degenerate, forming upper and lower polaritonic Dirac cones at energies of $E_\pm = \omega_p \pm \sqrt{|\alpha|^2 + |\beta|^2}$.

In addition to the four bright polariton bands, there are also two dark exciton bands with no photon components. To confirm the existence of polaritonic Dirac points (DPs), we calculate polaritonic band structures using the FDTD method, where the TMD monolayer is modeled as a dielectric material with Lorentz poles [20] in its

permittivity tensor $\bar{\bar{\varepsilon}}$ (see Supplemental Material [25] for details). The simulation result is shown in Fig. 2(d), which is in good agreement with the analytical result obtained from the effective Hamiltonian with the exciton-photon coupling strength ($|\alpha|$ and $|\beta|$) being fitting parameters. The observed Rabi splitting between the two DPs is $2\sqrt{|\alpha|^2 + |\beta|^2} = 28$ meV, which is comparable to experimental results obtained in similar settings of TMD-PhC polaritons [12,13,26].

Similar to DPs in two-dimensional electronic and photonic systems, the presence of polaritonic DPs are protected by the product of inversion and time-reversal symmetries. Therefore, breaking P or T lifts the degeneracies, leading to gapped phases with distinct bulk topologies. To break P, one can allow the two holes in a photonic unit cell to have different radii. This is equivalent to adding a mass term $m\sigma_z$ to the bare photonic Dirac cone and, consequently, gapping out both polaritonic Dirac points [Fig. 3(a)]. However, due to the presence of time-reversal symmetry, the resulting energy gaps are topologically trivial with zero Chern numbers (C), as can be confirmed by using the C_3 eigenvalues at high-symmetry $\mathbf{k}$ points of all bands below the energy gaps [27]: $e^{i2\pi C/3} = \prod_i c_{3,i}(\Gamma) c_{3,i}(K) c_{3,i}(K')$, where $c_{3,i}(K) = c_{3,i}^*(K')$ as required by T.

In contrast, the introduction of T-breaking perturbations by lifting the exciton valley degeneracy ($\omega_K \neq \omega_{K'}$ and $N_X = 2$) leads to distinct gapped energy spectrum with nontrivial bulk topology. One method to break T is to apply a perpendicular magnetic field that induces a valley Zeeman splitting [28–30]. Another effective approach is
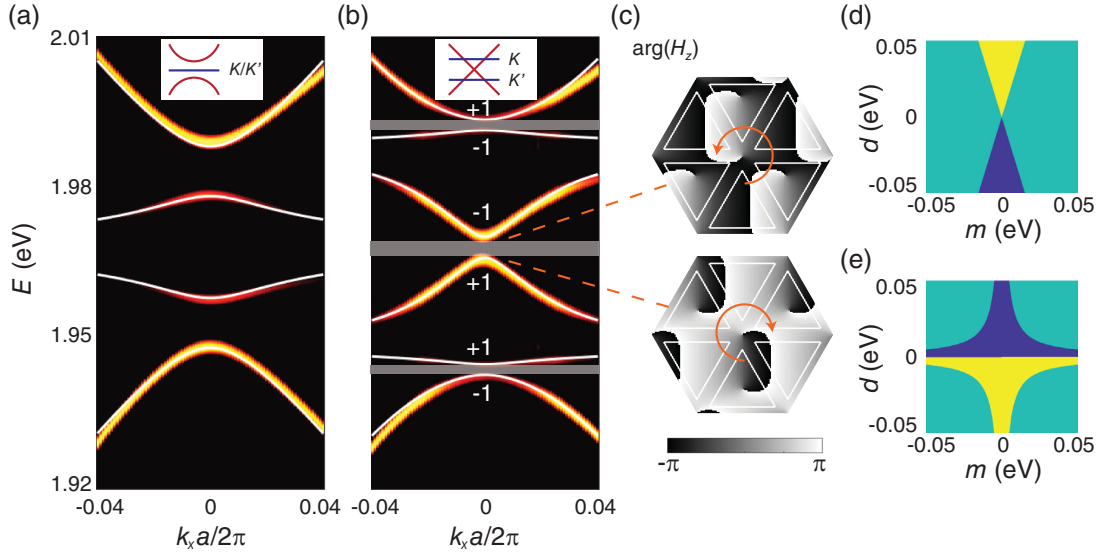
FIG. 3. Polaritonic topological phase transitions by lifting exciton valley degeneracy. (a) and (b) Breaking either P or T removes the degeneracies at K/K', leading to gapped polaritonic band structures with distinct bulk topology. In the P-breaking case (a), the two holes in a unit cell have different radii ($r_1 = 125$ and $r_2 = 135$ nm). In the T-breaking case (b), the exciton energies in K/K' valleys are shifted by $d = \pm 19.7$ meV with respect to ω_p. (c) H_z mode profiles for the third and fourth bands at K feature opposite phase winding of $\pm 2\pi$. (d) and (e) Topological phase diagrams for the first and third bulk energy gaps (shaded in gray) exhibit different phase transition boundaries. Yellow, $C = 1$; blue, $C = -1$; green, $C = 0$.

through the valley-selective optical Stark effect, where large valley exciton energy splitting up to tens of meV has been observed experimentally even at room temperature [31–33]. We note another possible method to achieve polariton Chern insulators is to first switch off the excitonic transition in one of the valleys [34]—requiring T to be broken—and then strongly couple to a photonic Dirac cone (see Supplemental Material [25]). However, none of these T-breaking mechanisms are required for the realization of symmetry-protected polariton phases [12,13]. When T is broken, the block degeneracy in the effective Hamiltonian is lifted, and all bands hybridize together to yield $2 \times (2 + 1) = 6$ polaritonic bands [Fig. 3(b)]. This is in contrast to the P-breaking case, where only four polariton bands are observed. Moreover, the presence of inversion symmetry relates the C_3 eigenvalues at K and K': $c_{3,i}(K) = c_{3,i}(K')$. This indicates that all the polariton bands have nonzero Chern numbers, which can be inferred directly from the phase winding in the H_z mode profiles at the K point [Fig. 3(c)]. Remarkably, the observed topological gap size of 4.1 meV induced by a TMD monolayer is at least an order of magnitude larger than that of semiconductor quantum well exciton polaritons [11], owing to the strong light-matter interactions in 2D TMDs. The topological phase diagrams for different energy gaps (shaded in gray) as a function of P- and T-breaking strengths are shown in Figs. 3(d) and 3(e). The distinct phase transition boundaries of the middle gap [Fig. 3(d)] as compared to the that of the bottom gap [Fig. 3(e)] are because the polariton bands above and below

the middle gap are dominated by exciton components, which are not affected by P-breaking perturbations.

Finally, we show the existence of polaritonic chiral edge states at the interfaces between a polaritonic Chern insulator and normal insulators. To this end, we consider a supercell geometry where a polaritonic Chern insulator is sandwiched between normal insulators that support a wide band gap for the energy range of interest. To further enhance the topological gap size and hence the visibility of the chiral edge states in our simulation, we increase the exciton density by considering multiple TMD monolayers coupled to the PhC slab [35,36] (the exciton-photon coupling strength and the resulting topological gap size is proportional to $\sqrt{N_{\text{layer}}}$, see Supplemental Material [25] for details). Figure 4 shows the projected dispersion of the
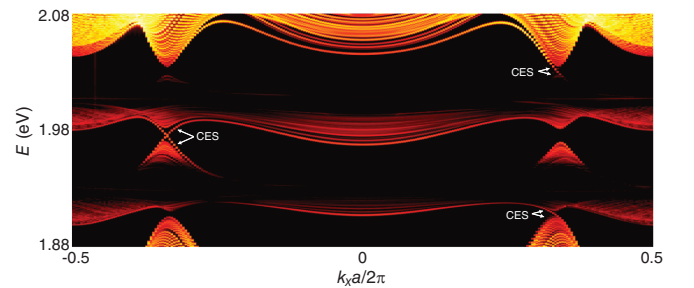

FIG. 4. Chiral edge states (CES) at the interfaces between a polaritonic Chern insulator and normal insulators. The normal insulators have a similar design as the P-breaking case in Fig. 3(a), with $r_1 = 75$ and $r_2 = 165$ nm. Further details of the supercell setup can be found in the Supplemental Material [25].

semi-infinite strip. Edge states emerge at both top and bottom interfaces with their energies traversing across all the three bulk topological gaps, which indicates the unidirectional nature of the edge modes.

Discussion.—In summary, our Letter reveals that the modified optical selection rules are indispensable when extending the study of exciton polaritons from free-space optics to nanophotonic structures. Incorporating this essential modification into our theoretical framework predicts topological exciton polaritons with completely new bulk topology and boundary manifestations. Using numerical calculations with realistic material parameters, we show large polaritonic topological gaps can be opened as a result of the strong light-matter interactions in 2D TMDs, featuring polaritonic chiral edge states inside the topological gaps. Note that our Letter is to be distinguished from previous experimental studies on symmetry-protected polariton phases [12,13] in that the time-reversal symmetry in our system is broken, leading to fundamentally different bulk topology and boundary manifestations. Our theoretical model, taking into account the variation of local field polarization in nanophotonic structures, predicts a number of topological properties of the exciton-polariton dispersions different from the conventional theory based on the plane wave approximation [9,11]. The predicted polaritonic chiral edge states can be readily observed by combining high-quality TMD monolayers [21] with low-loss dielectric PhC slabs, which may enable novel polaritonic devices with topological protection, such as polaritonic topological lasers, isolators, circulators, and unidirectional amplifiers. The presented theoretical analysis of collective coupling between excitons and photonic Bloch modes is applicable to a wide range of material platforms, such as quantum well microcavity exciton polaritons, and provides a comprehensive understanding of strongly coupled light-matter systems. Finally, combining with the strong nonlinearities of excitons in TMDs [16], TMD-PhC exciton polaritons may provide a fertile experimental test bed to explore nonlinear and interacting topological phenomena beyond single particle level.

*Corresponding author.
bozhen@sas.upenn.edu

[1] T. Byrnes, N. Y. Kim, and Y. Yamamoto, Exciton–polariton condensates, Nat. Phys. **10**, 803 (2014).

[2] A. Amo, J. Lefrère, S. Pigeon, C. Adrados, C. Ciuti, I. Carusotto, R. Houdré, E. Giacobino, and A. Bramati, Superfluidity of polaritons in semiconductor microcavities, Nat. Phys. **5**, 805 (2009).

[3] J. M. Kosterlitz and D. J. Thouless, Ordering, metastability and phase transitions in two-dimensional systems, J. Phys. C **6**, 1181 (1973).

[4] M. Z. Hasan and C. L. Kane, Colloquium: Topological insulators, Rev. Mod. Phys. **82**, 3045 (2010).

[5] L. Lu, J. D. Joannopoulos, and M. Soljačić, Topological photonics, Nat. Photonics **8**, 821 (2014).

[6] T. Ozawa, H. M. Price, A. Amo, N. Goldman, M. Hafezi, L. Lu, M. C. Rechtsman, D. Schuster, J. Simon, O. Zilberberg *et al.*, Topological photonics, Rev. Mod. Phys. **91**, 015006 (2019).

[7] T. Karzig, C.-E. Bardyn, N. H. Lindner, and G. Refael, Topological Polaritons, Phys. Rev. X **5**, 031001 (2015).

[8] C.-E. Bardyn, T. Karzig, G. Refael, and T. C. H. Liew, Topological polaritons and excitons in garden-variety systems, Phys. Rev. B **91**, 161413(R) (2015).

[9] A. V. Nalitov, D. D. Solnyshkov, and G. Malpuech, Polariton z Topological Insulator, Phys. Rev. Lett. **114**, 116401 (2015).

[10] K. Yi and T. Karzig, Topological polaritons from photonic Dirac cones coupled to excitons in a magnetic field, Phys. Rev. B **93**, 104303 (2016).

[11] S. Klembt, T. Harder, O. Egorov, K. Winkler, R. Ge, M. Bandres, M. Emmerling, L. Worschech, T. Liew, M. Segev *et al.*, Exciton-polariton topological insulator, Nature (London) **562**, 552 (2018).

[12] W. Liu, Z. Ji, Y. Wang, G. Modi, M. Hwang, B. Zheng, V. J. Sorger, A. Pan, and R. Agarwal, Generation of helical topological exciton-polaritons, Science **370**, 600 (2020).

[13] M. Li, I. Sinev, F. Benimetskiy, T. Ivanova, E. Khestanova, S. Kiriushechkina, A. Vakulenko, S. Guddala, M. Skolnick, V. M. Menon *et al.*, Experimental observation of topological $z2$ exciton-polaritons in transition metal dichalcogenide monolayers, Nat. Commun. **12**, 4425 (2021).

[14] Y. Sun, Y. Yoon, M. Steger, G. Liu, L. N. Pfeiffer, K. West, D. W. Snoke, and K. A. Nelson, Direct measurement of polariton–polariton interaction strength, Nat. Phys. **13**, 870 (2017).

[15] E. Togan, H.-T. Lim, S. Faelt, W. Wegscheider, and A. Imamoglu, Enhanced Interactions between Dipolar Polaritons, Phys. Rev. Lett. **121**, 227402 (2018).

[16] L. Zhang, F. Wu, S. Hou, Z. Zhang, Y.-H. Chou, K. Watanabe, T. Taniguchi, S. R. Forrest, and H. Deng, van der Waals heterostructure polaritons with moiré-induced nonlinearity, Nature (London) **591**, 61 (2021).

[17] L. He, Z. Addison, E. J. Mele, and B. Zhen, Quadrupole topological photonic crystals, Nat. Commun. **11**, 3119 (2020).

[18] P. Lodahl, S. Mahmoodian, S. Stobbe, A. Rauschenbeutel, P. Schneeweiss, J. Volz, H. Pichler, and P. Zoller, Chiral quantum optics, Nature (London) **541**, 473 (2017).

[19] D. Xiao, G.-B. Liu, W. Feng, X. Xu, and W. Yao, Coupled Spin and Valley Physics in Monolayers of mos 2 and Other Group-VI Dichalcogenides, Phys. Rev. Lett. **108,** 196802 (2012).

[20] Y. Li, A. Chernikov, X. Zhang, A. Rigosi, H. M. Hill, A. M. van der Zande, D. A. Chenet, E.-M. Shih, J. Hone, and T. F. Heinz, Measurement of the optical dielectric function of monolayer transition-metal dichalcogenides: MoS_2, $MoSe_2$, WS_2, and WSe_2, Phys. Rev. B **90,** 205422 (2014).

[21] Y. Zhou, G. Scuri, J. Sung, R. J. Gelly, D. S. Wild, K. De Greve, A. Y. Joe, T. Taniguchi, K. Watanabe, P. Kim *et al.*, Controlling Excitons in an Atomically Thin Membrane with a Mirror, Phys. Rev. Lett. **124,** 027401 (2020).

[22] M. Tavis and F. W. Cummings, Exact solution for an *n*-molecule–radiation-field Hamiltonian, Phys. Rev. **170,** 379 (1968).

[23] M. Gross and S. Haroche, Superradiance: An essay on the theory of collective spontaneous emission, Phys. Rep. **93,** 301 (1982).

[24] M. J. Collins, F. Zhang, R. Bojko, L. Chrostowski, and M. C. Rechtsman, Integrated optical Dirac physics via inversion symmetry breaking, Phys. Rev. A **94,** 063827 (2016).

[25] See Supplemental Material at http://link.aps.org/supplemental/10.1103/PhysRevLett.130.043801 for detailed discussion on numerical calculations.

[26] L. Zhang, R. Gogna, W. Burg, E. Tutuc, and H. Deng, Photonic-crystal exciton-polaritons in monolayer semiconductors, Nat. Commun. **9,** 713 (2018).

[27] C. Fang, M. J. Gilbert, and B. A. Bernevig, Bulk topological invariants in noninteracting point group symmetric insulators, Phys. Rev. B **86,** 115112 (2012).

[28] A. Srivastava, M. Sidler, A. V. Allain, D. S. Lembke, A. Kis, and A. Imamoğlu, Valley Zeeman effect in elementary optical excitations of monolayer WSe2, Nat. Phys. **11,** 141 (2015).

[29] G. Aivazian, Z. Gong, A. M. Jones, R.-L. Chu, J. Yan, D. G. Mandrus, C. Zhang, D. Cobden, W. Yao, and X. Xu, Magnetic control of valley pseudospin in monolayer WSe2, Nat. Phys. **11,** 148 (2015).

[30] P. D. Cunningham, A. T. Hanbicki, T. L. Reinecke, K. M. McCreary, and B. T. Jonker, Resonant optical Stark effect in monolayer WS_2, Nat. Commun. **10,** 5539 (2019).

[31] E. J. Sie, J. W. McIver, Y.-H. Lee, L. Fu, J. Kong, and N. Gedik, Valley-selective optical Stark effect in monolayer WS2, Nat. Mater. **14,** 290 (2015).

[32] J. Kim, X. Hong, C. Jin, S.-F. Shi, C.-Y. S. Chang, M.-H. Chiu, L.-J. Li, and F. Wang, Ultrafast generation of pseudo-magnetic field for valley excitons in WSe_2 monolayers, Science **346,** 1205 (2014).

[33] C.-K. Yong, M. Utama, C. S. Ong, T. Cao, E. C. Regan, J. Horng, Y. Shen, H. Cai, K. Watanabe, T. Taniguchi *et al.*, Valley-dependent exciton fine structure and Autler–Townes doublets from Berry phases in monolayer $MoSe_2$, Nat. Mater. **18,** 1065 (2019).

[34] T. Lyons, D. Gillard, C. Leblanc, J. Puebla, D. Solnyshkov, L. Klompmaker, I. Akimov, C. Louca, P. Muduli, A. Genco *et al.*, Giant effective Zeeman splitting in a monolayer semiconductor realized by spin-selective strong light–matter coupling, Nat. Photonics **16,** 632 (2022).

[35] S. Dufferwiel, S. Schwarz, F. Withers, A. Trichet, F. Li, M. Sich, D. Pozo-Zamudio, C. Clark, A. Nalitov, D. Solnyshkov *et al.*, Exciton–polaritons in van der Waals heterostructures embedded in tunable microcavities, Nat. Commun. **6,** 8579 (2015).

[36] J. Gu, B. Chakraborty, M. Khatoniar, and V. M. Menon, A room-temperature polariton light-emitting diode based on monolayer WS_2, Nat. Nanotechnol. **14,** 1024 (2019).